Bulletin of Mathematical Biology (2024) 86:53
https://doi.org/10.1007/s11538-024-01284-2

Society for Mathematical Biology

ORIGINAL ARTICLE

Mathematical Models of Early Hepatitis B Virus Dynamics in Humanized Mice

Stanca M. Ciupe[1] · **Harel Dahari**[2] · **Alexander Ploss**[3]

Received: 25 October 2023 / Accepted: 15 March 2024 / Published online: 9 April 2024

Abstract

Analyzing the impact of the adaptive immune response during acute hepatitis B virus (HBV) infection is essential for understanding disease progression and control. Here we developed mathematical models of HBV infection which either lack terms for adaptive immune responses, or assume adaptive immune responses in the form of cytolytic immune killing, non-cytolytic immune cure, or non-cytolytic-mediated block of viral production. We validated the model that does not include immune responses against temporal serum hepatitis B DNA (sHBV) and temporal serum hepatitis B surface-antigen (HBsAg) experimental data from mice engrafted with human hepatocytes (HEP). Moreover, we validated the immune models against sHBV and HBsAg experimental data from mice engrafted with HEP and human immune system (HEP/HIS). As expected, the model that does not include adaptive immune responses matches the observed high sHBV and HBsAg concentrations in all HEP mice. By contrast, while all immune response models predict reduction in sHBV and HBsAg concentrations in HEP/HIS mice, the Akaike Information Criterion cannot discriminate between non-cytolytic cure (resulting in a class of cells refractory to reinfection) and antiviral block functions (of up to 99% viral production 1–3 weeks following peak viral load). We can, however, reject cytolytic killing, as it can only match the sHBV and HBsAg data when we predict unrealistic levels of hepatocyte loss.

Keywords Mathematical modeling · HBV · HBsAg · Humanized mice

✉ Stanca M. Ciupe
stanca@vt.edu

1 Department of Mathematics, Virginia Polytechnic Institute and State University, Blacksburg, VA, USA

2 Division of Hepatology, Department of Medicine, Loyola University, Chicago, IL, USA

3 Department of Molecular Biology, Princeton University, Princeton, NJ, USA

1 Introduction

Our current understanding of key immunological interactions and molecular dynamics responsible for the early stages of hepatitis B virus (HBV) infection is largely based on mathematical modeling validated against virus titer data in the serum of infected patients and chimpanzees Ciupe et al. (2007b, 2014, 2007a); Murray et al. (2005); Forde et al. (2016). These models have provided information about early HBV dynamics and the potential role of immune system in viral clearance or establishment of chronic disease. They showed that resolution of acute infections, where high levels of up to 10^{10} HBV DNA copies per ml and potentially up to 95% infections in adults are spontaneously cleared within 3-6 months, requires a broad and vigorous adaptive immune response. However, the exact interplay and contribution of humoral and cellular immune responses remain unknown Ciupe (2018); Ferrari et al. (1990). The humoral immune response yields virus specific antibodies capable of neutralizing infectious HBV and can thereby protect hepatocytes from new infections Glebe et al. (2009); Rath and Devey (1988). Anti-HBV antibodies have been shown to play a role only in the final resolution on the infection Ciupe et al. (2014). By contrast, CD8 T cell-mediated immune responses have been shown to remove infected cells through cytolytic killing and permanently inactivating HBV in cells through non-cytolytic mechanisms (such as the production of cytokines) McClary et al. (2000); Guidotti et al. (1996); Wieland et al. (2004). Such cellular adaptive immune responses have been shown to play a role in both controlling overall viremia and contributing to HBV clearance Ciupe et al. (2007b); Murray et al. (2005); Ciupe et al. (2007a). Notably, modeling work postulates that virus resolution through non-cytolytic mechanisms requires that cured cells remain refractory to reinfection by the (still) abundant virus Ciupe et al. (2007a). Lastly, mathematical models have shown that the size of inoculum dose has an effect on both the timing of the CD8 T cell expansion and the quality of its response, especially its non-cytolytic function Ciupe et al. (2021), hence explaining the observed relationship between inoculum size and infection outcome in HBV-infected chimpanzees Asabe et al. (2009).

Despite these advances, the lack of immunological and molecular data in the early acute phase of the infection has hampered our understanding of the mechanistic interactions that determine successful viral expansion, infection outcome, and (later on) treatment response. The intricate interplay between the virus and the immune system requires quantification of additional data on viral markers such as serum hepatitis B surface-antigen (HBsAg), serum hepatitis B e-antigen (HBeAg), serum HBV DNA (sHBV), various HBV nucleic acid replication intermediates - covalently closed circular DNA(cccDNA), intracellular HBV DNA, pre-genomic RNA (pgRNA) - as well as phenotyping and functional testing of antiviral T cell responses.

The recent establishment of humanized mice, i.e. mice expressing human genes and/or engrafted with human tissue, has provided access to early measurements of virological and molecular markers. Mice are either singly engrafted with human hepatocytes (HEP) Hogan et al. (2023); Gutti et al. (2014); Dusséaux et al. (2017) or dually co-engrafted with human hepatocytes and components of a human immune system (HEP/HIS) Hogan et al. (2023); Billerbeck et al. (2016); Dusséaux et al. (2017) before being challenged with HBV. The humanized human liver provides the neces-

sary environment for HBV, a uniquely human-, hepatotropic virus. Co-engraftment of components of a human immune system enables tracking of human immunity in responses to the viral infection in the liver. In this study, we analyzed data from two groups of either HEP or HEP/HIS mice challenged with HBV for which longitudinal sHBV and longitudinal HBsAg titers were collected biweekly for up to six weeks following infection Hogan et al. (2023). HBsAg is believed to serve as both decoy against humoral immune responses Ciupe et al. (2014) and to induce T-cell exhaustion Kim et al. (2020); Fang et al. (2015); Bertoletti and Gehring (2006). Mice in the HEP/HIS group had lower sHBV and HBsAg levels than HEP mice, suggesting that the grafted human immune system mounts an antiviral response, which can, at least partially, control HBV infection Hogan et al. (2023). Several mechanisms may explain the observed differences: either (partial) loss/death of productively HBV-infected cells i.e. cytolytic killing or non-cytolytic suppression of HBV replication. In case of cytolytic elimination of HBV infection, immune inflicted liver damage would trigger proliferation of naÃ¯ve hepatocytes, which in turn could be targets for *de novo* infection by circulating HBV, thereby establishing a dynamic equilibrium. To explore the mechanisms or combined mechanisms responsible for the observed differences in the sHBV and HBsAg dynamics in the HEP and HEP/HIS groups, we developed mathematical models of HBV infection and validated them against sHBV and HBsAg titer data.

2 Mathematical Model

We utilized a within-host model of HBV infection that considers the interaction between target liver cells, T, infected liver cells, I, HBV, V, and HBsAg, S, as follows Ciupe et al. (2007b, a); Kadelka et al. (2021). Target cells, T, interact with the virus, V, at rate β to become infected cells, I. Infected cells die at per capita rate δ, and produce virus at rate p. Virus is cleared at rate c. Uninfected cells are maintained through homeostasis. We model this using a logistic term with maximum per capita growth rate r and carrying capacity K. Lastly, HBsAg, S are produced at rate r_S (proportional to the infected cell density) and decay at per capita rate d_S. The diagram describing these interactions is shown in Fig. 1A and the interactions are given by the following system,

$$\begin{aligned}
\frac{dT}{dt} &= rT(1 - \frac{T+I}{K}) - \beta TV, \\
\frac{dI}{dt} &= \beta TV - \delta I, \\
\frac{dV}{dt} &= pI - cV, \\
\frac{dS}{dt} &= r_S I - d_S S,
\end{aligned} \tag{1}$$

with initial conditions $T(0) = K$, $I(0) = 0$, $V(0) = V_0$ and $S_0 = S_0$. We use model Eq. 1 to understand the mechanistic interactions responsible for the differences between HBV infections in HEP and HEP/HIS mice.

3 Data Fitting

3.1 Empirical Data

Humanized mice were generated by engrafting human hepatocytes (HEP mice) or hepatocytes and human immune cells (HEP/HIS mice) into immunodeficient xenorecipient strains (for details please see Hogan et al. (2023)). Human hepatic and/or hematopoietic engraftment was quantified prior to infection with HBV. Groups of HEP mice (n = 7) and HIS/HEP mice (n = 12) were infected intravenously with cell-culture produced HBV (1x10E6 GE/mouse, genotype D, strain ayw). Blood was sampled prior to and at weeks 2, 4 and 6 post infection. At week 6, all mice were culled to harvest blood, spleens and livers for analysis. Several virological markers (HBeAg, HBsAg, sHBV) as well as human albumin was quantified in the serum by ELISA and qPCR. HBV DNA, pgRNA, and cccDNA were quantified in liver tissue by (RT)qPCR. Frequencies and phenotypes of human lymphocytes were measured in the blood, spleens and livers by flowcytometry Hogan et al. (2023). For the modeling purposes we only used sHBV and HBsAg titers, for which we have temporal data above limit of detection.

3.2 Parameter Estimation

We assume that $K = 6.8 \times 10^5$ hepatocytes/ml are susceptible to HBV infection (20-times lower than in humans Ciupe et al. (2007a)), their per capita division rate is $r = 1$ per day Ciupe et al. (2007b), virus is cleared at rate $c = 4.4$ per day Murray et al. (2006), and HBsAg decays at rate $d_S = 0.01$ per day Kadelka et al. (2021). The initial conditions are $T(0) = K$ per ml, $I(0) = 0$ per ml, $V(0) = 100$ per ml (the virus limit of detection) and $S(0) = 10^{-6}$ per ml (below the HBsAg limit of detection). For the mice in the HEP group (i.e. without human immune response) we estimate parameters $par_{HEP} = \{\beta, r_S, p\}$ by fitting theoretical curves for $V(t)$ and $S(t)$ as given by Eq. 1 with $\delta = 0$ to sHBV and HBsAg empirical data. For the mice in the HEP/HIS group, we estimate parameters $par_{HEP/HIS} = \{\beta, r_S, \delta, p\}$ by fitting theoretical curves for $V(t)$ and $S(t)$ as given by Eq. 1 to sHBV and HBsAg empirical data. For a description of model parameters see Table 1.

3.3 Fitting Method

We validate model Eq. 1 against individual mouse sHBV and HBsAg data in either the HEP or HEP/HIS mouse groups, as follows. We estimate unknown parameters par_{HEP} by fitting both $V(t)$ and $S(t)$ given by Eq. 1 with $\delta = 0$ to the individual HEP mouse sHBV and HBsAg data, simultaneously. We estimate unknown parameters $\mathbf{par}_{HEP/HIS}$ by fitting both $V(t)$ and $S(t)$ given by Eq. 1 with $\delta \neq 0$ to the individual HEP/HIS mouse sHBV and HBsAg data, simultaneously. We define the objective functional

Table 1 Parameters description

Parameter	Description	Value	References
r	Hepatocyte division rate	1 d^{-1}	Ciupe et al. (2007b)
K	Hepatocyte carrying capacity	6.8×10^5 hep/ml	Ciupe et al. (2007a)
β	Infectivity rate	estimated	–
δ	Killing rate	estimated	–
p	Viral production rate	estimated	–
c	Virus clearance rate	4.4 d^{-1}	Murray et al. (2005)
ρ	Recovery rate	0.05 d^{-1}	–
η	Waning rate	0.001 d^{-1}	Ciupe et al. (2007a)
r_S	HBsAg production rate	estimated	–
d_S	HBsAg decay rate	0.01 d^{-1}	Kadelka et al. (2021)

Initial Condition	Description	Value	Reference
$T(0)$	Healthy hepatocytes	K hep/ml	–
$I(0)$	Infected hepatocytes	0 hep/ml	–
$R(0)$	Recovered hepatocytes	0 hep/ml	- -
$V(0)$	Initial virus	100 virion/ml	–
$S(0)$	Initial HBsAg	10^{-6} HBsAg/ml	–

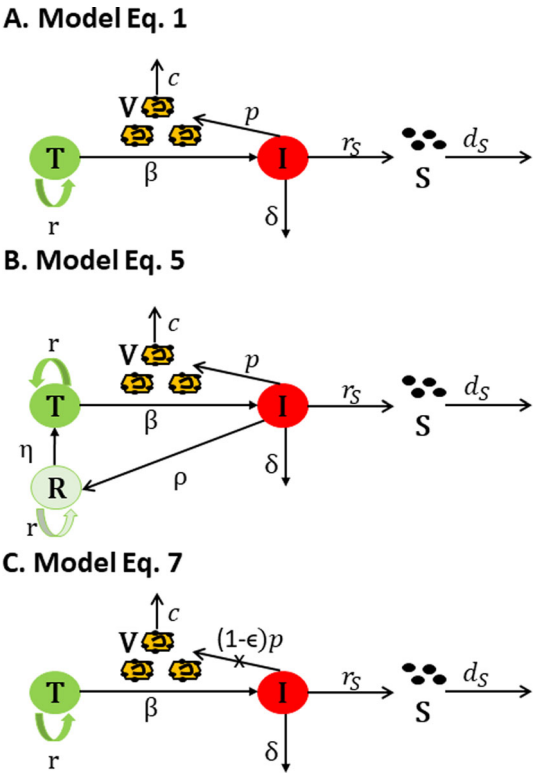

Fig. 1 Model description. **A**: Model of HBV infection with cytotoxic immune responses given by Eq. 1; **B**. Model of HBV infection with non-cytotoxic immune responses given by Eq. 6; and **C**: Model of HBV infection with antiviral effects given by Eq. 8

$$J(\mathbf{par_n}) = \left(\sum_{\mathbf{j=1}}^{\mathbf{4}} (\log_{\mathbf{10}} \mathbf{V^i(j)} - \log_{\mathbf{10}} \mathbf{V_d^i(j)}\right)^{\mathbf{1/2}} + \left(\sum_{j=1}^{4} (\log_{10} S^i(j) - \log_{10} S_d^i(j))^2\right)^{1/2}, \tag{2}$$

for each animal i. Here $V(j)$ is the virus curve given by model Eq. 1 at day j post infection, $V_d(j)$ is the sHBV data at day j post infection, $S(j)$ is the HBsAg curve given by model Eq. 1 at day j post infection, $S_d(j)$ is the HBsAg data at day j post infection, $j = \{0, 14, 28, 42\}$ days, and $n = \{\text{HEP, HEP/HIS}\}$. We minimize $J(\mathbf{par_n})$ over the parameter space using the *fminsearch* function in MATLAB. The results for the HEP mice are shown in Fig. 2A, B and the best parameter fits are given in Table 2. Similarly, the results for the HEP/HIS mice are shown in Fig. 2C, D and the best parameter fits are given in Table 3.

Additionally, to address heterogeneity in the HEP/His data, we estimate population level mean and standard deviation for parameters $\mathbf{p} = \{\beta, r_S, \delta, p\}$ for model Eq. 1 using a non-linear mixed effects modelling approach that utilizes Stochastic Approximation Estimation-Maximization (SAEM) algorithm in Monolix Monolix version 2019r2 (2019) (see Fig. S1 and table S1).

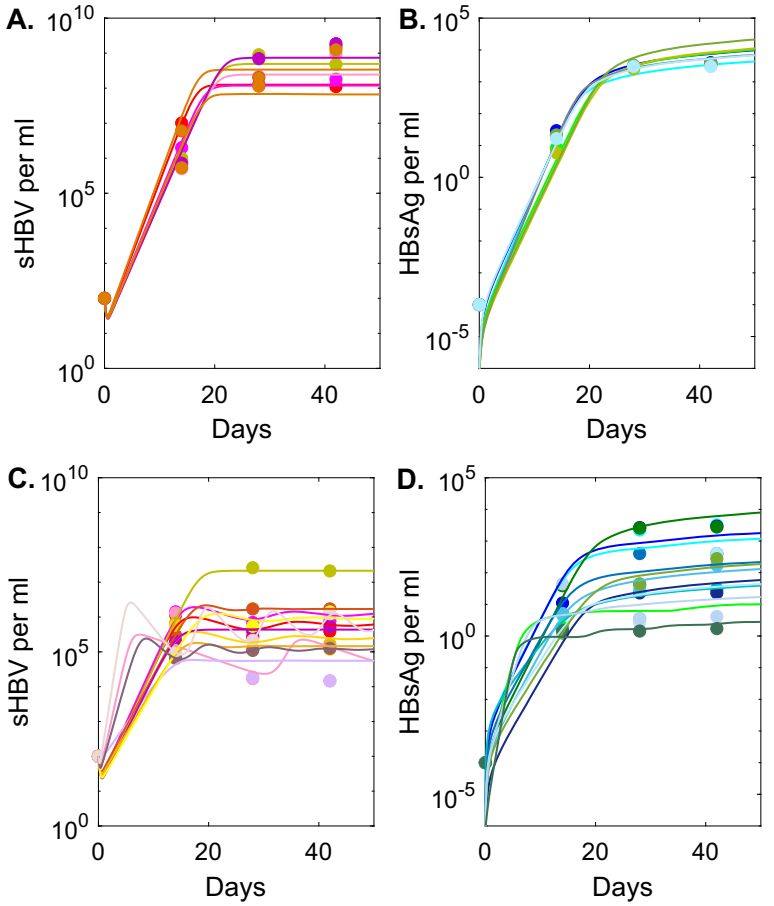

Fig. 2 **A**, **B**: $V(t)$ and $S(t)$ as given by model Eq. 1 with $\delta = 0$ versus HEP data; **C**, **D**: $V(t)$ and $S(t)$ as given by model Eq. 1 with $\delta \neq 0$ versus HEP/HIS data. Model parameters are given in Table 3 (Color figure online)

4 Results

4.1 Analytical Results

Model Eq. 1 has three equillibria, the no-liver equilibrium

$$E_0 = (0, 0, 0, 0),$$

which is not biologically realistic; the disease free equilibrium

$$E_1 = (K, 0, 0, 0),$$

Table 2 Parameter estimates found by fitting model Eq. 1 with $\delta = 0$ to sHBV and HBsAg data for the HEP group

HEP group Eq. 1 $\delta = 0$				
mouse id	$\beta \times 10^{-9}$ ml/(vir.× d)	$r_S \times 10^{-4}$ 1/(inf. cell× d)	p 1/(inf. cell× d)	RSS
229	9.24	2.24	813	0.3
14045	8.83	5.23	768	0.73
14055	4.0	5.74	1580	1.26
14056	2.0	6.42	3190	0.93
14058	3.6	3.65	2190	1.04
14064	1.3	13	4790	1.7
14068	14.8	3.71	448	1.73
mean	6.27	5.71	1970	
median	4.04	5.23	1580	

Table 3 Parameter estimates found by fitting model Eq. 1 with $\delta \neq 0$ to sHBV and HBsAg data for the HEP/HIS group

HEP/HIS group Eq. 1, $\delta \neq 0$					
mouse id	$\beta \times 10^{-7}$ ml/(vir.× d) ml/(vir.× d)	$r_S \times 10^{-4}$ 1/(inf. cell× d) 1/(inf. cell× d)	δ 1/d 1/d	p 1/(inf. cell× d) 1/(inf. cell× d)	RSS
3205	7.27	1.33	0.155	9.8	1.78
3206	3.77	2.09	0.172	19.8	1.26
3346	62.1	0.01	0.126	2.54	1.85
14051	0.43	4.24	0	138	0.67
14062	26.8	1.09	7.46	21.6	1.54
8061	2.00	0.14	0.775	54.7	0.46
8044	17.1	0.24	0.157	3.85	1.71
669	19.7	0.06	0	2.82	0.49
621	22.8	0.09	0.599	3.96	1.49
623	4.23	0.23	0.203	14.6	0.62
661	46.2	0.03	0.501	3.25	1.2
612	10.0	0.006	0.473	27.8	0.33
mean	18.5	0.79	0.18	25.3	
median	13.6	0.18	0.18	12.2	

and the endemic equilibrium

$$E_2 = \left(\frac{c\delta}{\beta p}, \frac{r - \frac{c\delta r}{\beta pK}}{\frac{r}{K} + \beta \frac{p}{c}}, \frac{p(r - \frac{c\delta r}{\beta pK})}{c(\frac{r}{K} + \beta \frac{p}{c})}, \frac{r_S(r - \frac{c\delta r}{\beta pK})}{d_S(\frac{r}{K} + \beta \frac{p}{c})} \right),$$

Table 4 Parameter estimates found by fitting model Eq. 6 with $\rho = 0.05$ per day to sHBV and HBsAg data for the HEP/HIS group

HEP/HIS group					
mouse id	$\beta \times 10^{-7}$ ml/(vir.× d)	$r_S \times 10^{-4}$ 1/(inf. cell× d)	δ 1/d	p 1/(inf. cell× d)	RSS
3205	2.27	2.65	0.07	29.3	1.76
3206	3.27	1.96	0	20.3	1.25
3346	15	0.02	0.11	6.02	1.51
14051	0.23	6.72	0	290	0.76
14062	7.18	0.12	0.26	10.8	1.17
8061	3.04	0.04	0	21.5	0.68
8044	4.86	0.46	0.09	13.4	1.57
669	8.64	0.12	0	7.1	0.82
621	21.5	0.04	0	2.5	1.74
623	4.11	0.18	0	12.5	0.90
661	60	0.01	0	2.4	1.76
612	10.0	0.003	0.02	16.9	1.62
mean	26.7	1.0	0.05	36.2	
median	7.9	0.12	0.00002	13.2	

which exists iff and only if

$$R_0 = K\frac{\beta p}{c\delta} > 1.$$

Proposition 1 *The disease free equilibrium E_1 is locally asymptotically stable iff $R_0 < 1$ and unstable otherwise.*

Proof The Jacobian of Eq. 1 at equilibrium $\bar{E} = (\bar{T}, \bar{I}, \bar{V}, \bar{S})$ is

$$J(\bar{E}) = \begin{pmatrix} r - \frac{r}{K}\bar{I} - 2\frac{r}{K}\bar{T} - \beta\bar{V} & -\frac{r}{K}\bar{T} & -\beta\bar{T} & 0 \\ \beta\bar{V} & -\delta & \beta\bar{T} & 0 \\ 0 & p & -c & 0 \\ 0 & r_S & 0 & -d_S \end{pmatrix}.$$

The Jacobian evaluated at E_1 becomes

$$J(E_1) = \begin{pmatrix} -r & -r & -\beta K & 0 \\ 0 & -\delta & \beta K & 0 \\ 0 & p & -c & 0 \\ 0 & r_S & 0 & -d_S \end{pmatrix},$$

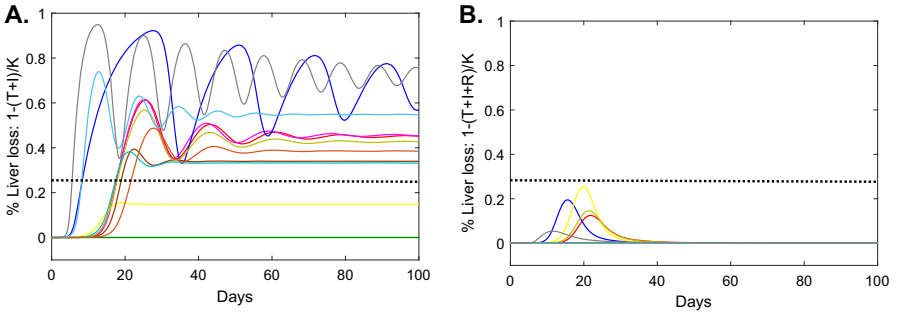

Fig. 3 **A**: Total liver loss $1-(T+I)/K$ predicted by model Eq. 1 with $\delta \neq 0$ for the HEP/HIS group; **B**: Total liver loss $1-(T+I+R)/K$ predicted by model Eq. 6 for the HEP/HIS group. Model parameters are given in Tables 3 and 4. Dashed black line accounts for an arbitrary chosen liver loss level of 30%, which we assume to be non-life threatening (Color figure online)

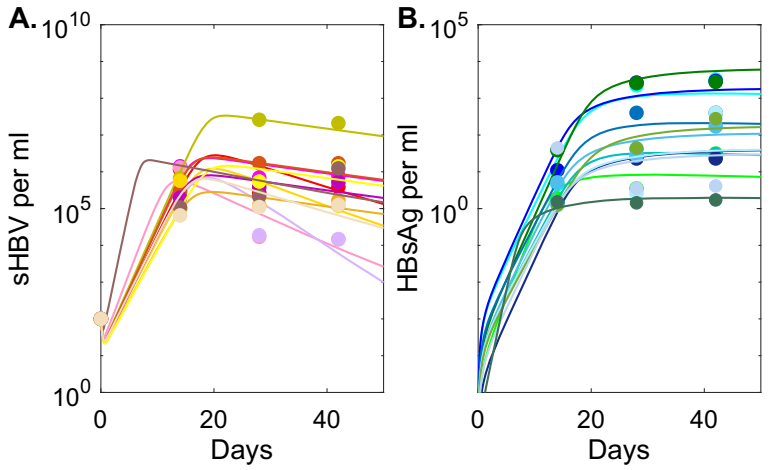

Fig. 4 **A**: $V(t)$ as given by model Eq. 6 versus HEP/HIS sHBV data; **B** $S(t)$ as given by model Eq. 6 versus HEP/HIS HBsAg data. Model parameters are given in Table 4 and $\rho = 0.05$ per day (Color figure online)

with eigenvalues $\lambda_1 = -d_S < 0$, $\lambda_2 = -r$, and

$$\lambda_{3,4} = \frac{-(c+\delta) \pm \sqrt{(c+\delta)^2 - 4(c\delta - \beta pK)}}{2} < 0$$

iff $R_0 = K\frac{\beta p}{c\delta} < 1$. Hence, equilibrium E_1 is locally asymptotically stable if $R_0 < 1$ and unstable otherwise. □

Proposition 2 *The endemic equilibrium E_2 is locally asymptotically stable if $R_0 > 1$ and $(\delta^2 + (3c+r)\delta + c^2)(\delta R_0 + r)R_0 + c(r^2 - R_0^3\delta^2) > 0$ and unstable otherwise.*

Proof The Jacobian of Eq. 1 evaluated at E_2

$$J(E_2) = \begin{pmatrix} -\frac{r}{R_0} & -\frac{r}{R_0} & -\frac{c\delta}{p} & 0 \\ \frac{r\delta(R_0-1)}{r\delta+R_0} & -\delta & \frac{c\delta}{p} & 0 \\ 0 & p & -c & 0 \\ 0 & r_S & 0 & -d_S \end{pmatrix},$$

has eigenvalues $\lambda_1 = -d_S < 0$ and $\lambda_{2,3,4}$ which solve the equation

$$\lambda^3 + A_1\lambda^2 + A_2\lambda + A_3 = 0,$$

with

$$\begin{aligned} A_1 &= c + \delta + \frac{r}{R_0}, \\ A_2 &= \frac{(\delta(c + r + \delta)R_0 + cr)r}{R_0(R_0\delta + r)}, \\ A_3 &= \frac{(R_0 - 1)c\delta r}{R_0}. \end{aligned} \tag{3}$$

By the Routh Hurwitz condition, eigenvalues $\lambda_{2,3,4}$ have negative real part if $A_1 > 0$ (always true), $A_2 > 0$ (always true), $A_3 > 0$ (true when $R_o > 1$) and $A_1A_2 - A_3 > 0$. It is easy to show that $A_1A_2 - A_3 > 0$ when $(\delta^2 + (3c + r)\delta + c^2)(\delta R_0 + r)R_0 + c(r^2 - R_0^3\delta^2) > 0$. This concludes our proof. □

Hence, in the long-run virus $V(t)$ and antigen $S(t)$ given by system Eq. 1 will either

1. Asymptotically reach zero, symbolizing clearance of infection, if $R_0 < 1$;
2. Reach the endemic equilibrium E_2 when $R_0 > 1$ and $(\delta^2 + (3c + r)\delta + c^2)(\delta R_0 + r)R_0 + c(r^2 - R_0^3\delta^2) > 0$;
3. Oscillate around the chronic equilibrium E_2 when $R_0 > 1$ and $(\delta^2 + (3c + r)\delta + c^2)(\delta R_0 + r)R_0 + c(r^2 - R_0^3\delta^2) < 0$.

4.2 Numerical Results

We found homogeneous dynamics within the HEP group for both sHBV (see Fig. 2A) and HBsAg (see Fig. 2B) curves. We predict low viral infectivity rate $\beta = 6.3 \times 10^{-9}$ ml/virus per day and large viral production $p = 1970$ virion per day. The HBsAg expansion rate is similar among the mice, with average $r_S = 5.7 \times 10^{-4}$ HBsAg being produced per infected cell per day.

By contrast, both sHBV and HBsAg dynamics within the HEP/HIS mice are more heterogeneous (see Fig. 2C and D), with mice 14051 and 669 having no indication of infected cell death $\delta = 0$ per day and the rest having an average infected cell killing rate $\delta = 0.18$ per day, corresponding to infected cell life-span of 5.5 days. The viral infectivity rate $\beta = 1.85 \times 10^{-6}$ ml/virus per day is 296-times higher than that of HEP group, but the average viral production $p = 25.3$ virion per day, is 77-times

Table 5 Parameter estimates found by fitting model Eq. 8 to sHBV and HBsAg data for the HEP/HIS group

HEP/HIS group mouse id	$\beta \times 10^{-7}$ ml/(vir.× d)	$r_S \times 10^{-4}$ 1/(inf. cell× d)	ϵ_0	τ d	p 1/(inf. cell× d)	RSS
3205	0.43	1.75	0.99	25.6	141	0.51
3206	1.12	1.50	0.91	25.5	57	0.53
3346	8.15	0.01	0.98	14	9.1	0.56
14051	0.43	4.24	0.00	0	138	0.63
14062	1.94	0.16	0.98	15	28	0.45
8061	4.99	0.03	0.58	48	11	0.46
8044	6.63	0.15	0.91	25.5	9.2	0.9
669	12.6	0.06	0.63	5.2	7.9	0.46
621	7.75	0.07	0.79	13.9	6.2	1.25
623	1.60	0.36	0.70	10.6	35.1	0.53
661	10.0	0.006	0.99	11.6	84.6	1.38
612	10.0	0.001	0.99	11	169	1.07
mean	6.88	0.7	0.79	17.2	58.1	
median	5.81	0.1	0.91	13.9	31.6	

lower. The HBsAg expansion rate varies among the HEP/HIS mice, with the average $r_S = 0.8 \times 10^{-4}$ HBsAg per infected cell per day, 6.7-times lower than that of the HEP mice.

For the ten mice in the HEP/HIS group for which the killing rate is non-zero, we computed the basic reproduction number

$$R_0 = K\frac{\beta p}{c\delta}, \tag{4}$$

which accounts for the average number of secondary cell infections in a naive hepatocyte population. The average basic reproduction number is $R_0 = 5.26$ (ranging between $R_0 = 1.02$ and $R_0 = 7.74$ among the ten mice) which is similar to the R_0 estimate in humans Whalley et al. (2001).

To determine the amount of liver damage due to immune mediated killing in the HEP/HIS group, we computed the total liver loss

$$Loss = 1 - \frac{T + I}{K}, \tag{5}$$

for the HEP/HIS group and found that a peak $38 - 95\%$ liver loss occurs in 9 out of 12 mice (see Fig. 3A), with mouse 62 experiencing 95% liver loss at day 12. The liver size does not rebound to its maximum in spite of the assumed liver proliferation. Interestingly, the amount of liver loss does not correlate with the magnitude of killing rate δ, but correlates weakly with R_0 (correlation coefficient $r = 0.79$ with p<0.006).

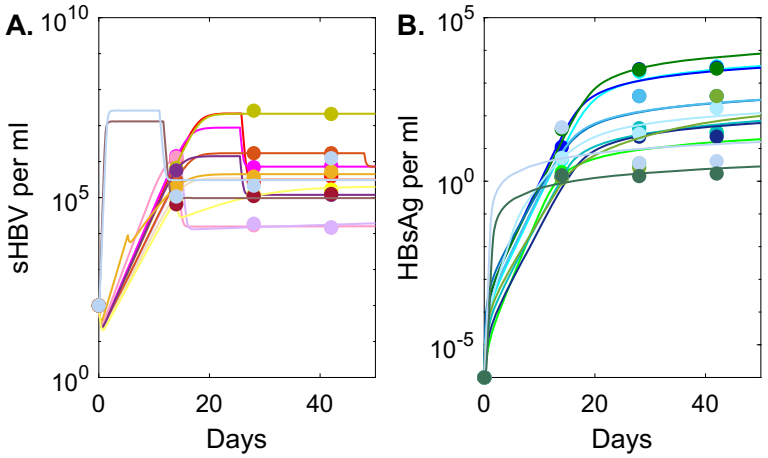

Fig. 5 **A**: $V(t)$ as given by model Eq. 8 versus HEP/HIS sHBV data; **B** $S(t)$ as given by model Eq. 8 versus HEP/HIS HBsAg data. Model parameters are given in Table 5 (Color figure online)

Since the large amount of liver killing predicted by model Eq. 1 in some of the HEP/HIS mice would lead to the animal's death and is, therefore, not realistic, we will next investigate alternative anti-viral effects, namely non-cytolytic immune responses that lead to cure and refraction state in the previously infected hepatocyte and non-cytolytic effects that lead to reduction in either viral infection or viral production. We will adjust model Eq. 1 to account for these two assumptions.

4.3 Refractory Cell Formation Following Cure in HEP/HIS Group

We modified model Eq. 1 by considering that cure of infected cells at rate ρ results in a class of immune and refractory to reinfection liver cells, R Ciupe et al. (2007a). Refractory cells proliferate at rate r (same as the uninfected cells), and the carrying capacity for this class is K (same as the uninfected cells). Refractory state wanes at rate η. These extended mechanisms are shown in Fig. 1B and the interactions are modeled in the following system,

$$\begin{aligned}
\frac{dT}{dt} &= rT(1-\frac{T+I+R}{K}) - \beta TV + \eta R,\\
\frac{dI}{dt} &= \beta TV - \delta I - \rho I,\\
\frac{dV}{dt} &= pI - cV,\\
\frac{dR}{dt} &= rR(1-\frac{T+I+R}{K}) + \rho I - \eta R,\\
\frac{dS}{dt} &= r_S I - d_S S,
\end{aligned} \tag{6}$$

with initial conditions $T(0) = K$, $I(0) = 0$, $R(0) = 0$, $V(0) = V_0$ and $S_0 = S_0$.

In the absence of data regarding maximum liver infection, we fixed the recovery rate to $\rho = 0.05$ per day, corresponding to a time in infected class before recovery of 20 days and set waning rate to $\eta = 0.001$ per day Ciupe et al. (2007a). We estimated individual mouse parameters $\mathbf{p}_{HEP/HIS} = \{\beta, r_S, \delta, p\}$ by fitting model Eq. 6 to HEP/HIS data, as before. Moreover, we estimated population level mean and standard deviation using a non-linear mixed effects modelling approach (see Fig. S2 and table S2). We found similar estimates as those of model Eq. 1 (with $\delta \neq 0$) for the infectivity rate β, the viral production rate p and the HBsAg production rate r_S. The infected cell death rate δ, however, is reduced on average 3.6-times, with seven out of twelve HEP/HIS mice experiencing no liver loss, $\delta = 0$ (see Table 4).

We computed the total liver loss for model Eq. 6,

$$Loss = 1 - \frac{T + I + R}{K}, \tag{7}$$

and found no liver loss in seven mice and transient liver loss in the other five. For these mice, maximum liver loss of $11 - 25\%$ occurred $11 - 21$ days post infection before the total hepatocyte population returned to maximum values K (see Fig. 3B).

We found similar dynamics for the HBsAg among models Eq. 1 (with $\delta \neq 0$) and Eq. 6, with equilibrium values of $2.7 - 7.8 \times 10^3$ copies per ml for model Eq. 1 and $2.7 - 6 \times 10^3$ copies per ml for model Eq. 6 (see Fig. 2D versus Fig. 4B). The dynamics of sHBV, however, differ among the two models. While sHBV reaches equilibrium values $4.3 \times 10^5 - 2.3 \times 10^7$ copies per ml that are close to the value of the virus peak for model Eq. 1 (see Fig. 2C), it drops to low equilibria $10^3 - 8.33 \times 10^5$ copies per ml (on average one year after infection) for model Eq. 6 (see Fig. 4A).

4.4 Antiviral Effects in the HEP/HIS Group

We modify model Eq. 1 by considering an immune-mediated antiviral response that reduces HBV production rate in the HEP/HIS group at a non-constant rate $\epsilon(t)$ in the absence of hepatocyte killing, $\delta = 0$. This mechanism is shown in Fig. 1C and the interactions are modeled by the following system,

$$\begin{aligned}
\frac{dT}{dt} &= rT(1 - \frac{T + I}{K}) - \beta TV, \\
\frac{dI}{dt} &= \beta TV, \\
\frac{dV}{dt} &= (1 - \epsilon(t))pI - cV, \\
\frac{dS}{dt} &= r_S I - d_S S,
\end{aligned} \tag{8}$$

Table 6 AIC values for models Eq. 6 and Eq.8. Emphasized values represent the best model for that subject. Results for mice for which bold and italic values are highlighted are inconclusive

HEP/HIS group		
mouse id	AIC for Eq. 6	AIC for Eq. 8
3205	−2.11	**−10.02**
3206	−4.85	**−9.71**
3346	−3.34	**−9.27**
14051	*−8.83*	*−8.33*
14062	−5.38	**−11.02**
8061	−9.72	**−10.85**
8044	−3.03	**−5.48**
669	−8.22	**−10.85**
621	*−2.20*	*−2.85*
623	−7.48	**−9.71**
661	*−2.11*	*−2.06*
612	−2.78	**−4.09**

where

$$\epsilon(t) = \begin{cases} 0, & t < \tau \\ \epsilon_0, & t \geq \tau \end{cases} \tag{9}$$

and initial conditions are $T(0) = K$, $I(0) = 0$, $V(0) = V_0$ and $S_0 = S_0$.

We assume that parameters r, c, d_S are known (see Section 3.2) and estimated individual mouse parameters $\mathbf{p}_{HEP/HIS} = \{\beta, r_S, p, \epsilon_0, \tau\}$ by fitting model Eq. 8 to HEP/HIS data, as before. Moreover, we estimated population level mean and standard deviation using a non-linear mixed effects modelling approach (see Fig. S3 and table S3). We found an average 79% reduction in viral production, occurring on average 17 days post infection (see Table 5). This leads to up to three order of magnitude reduction between peak and set points for mouse 661 and mouse 612, for which 99% antiviral effect occurred 11 days post infection. For mouse 3205, for which 99% reduction in viral production occurred at day 25 post infection, there was only a 36-fold decay from sHBV peak to set point (see Fig. 5A). Lastly, for mouse 14051 no reduction in the viral production is observed. The HBsAg dynamics do not change compared to the previous two models (see Fig. 5B), with average r_S values similar to those in models Eq. 1 and Eq. 6.

We also considered an antiviral effect that reduces virus infectivity rate β at non-constant rate $\sigma(t)$ in the absence of hepatocyte killing $\delta = 0$. It is given by

$$\begin{aligned} \frac{dT}{dt} &= rT(1 - \frac{T+I}{K}) - (1-\sigma(t))\beta TV + \rho I, \\ \frac{dI}{dt} &= (1-\sigma(t))\beta TV - \rho I, \\ \frac{dV}{dt} &= pI - cV, \\ \frac{dS}{dt} &= r_S I - d_S S, \end{aligned} \tag{10}$$

where

$$\sigma(t) = \begin{cases} 0, & t < \theta \\ \sigma_0, & t \geq \theta. \end{cases} \tag{11}$$

Model Eq. 10, however, did not fit the data well, having high residual sums of square (RSS) values for all mice. We, therefore, will not present them here.

4.5 Model Selection

Given that under realistic biological conditions (reduced liver killing) we have two models describing different immune mechanisms for the HEP/HIS data (Eq. 6 and Eq. 8), we computed Akaike Information Criterion (AIC) values for both in order to determine which model best describes the data. We let

$$AIC = n \ln(\frac{1}{n} \times RSS) + 2(k+1), \tag{12}$$

where n is the number of data points used for data fitting and k is the number of parameters being estimated. For both models $n = 8$ and $k = 4$ for Eq. 6, $k = 5$ for Eq. 8. Model selection theory says that a model with the lowest AIC best describes the data. We found that model Eq. 8 outperforms model Eq. 6 for nine mice (see Table 6 highlighted Italic). For the other three mice, however, the AIC values are similar (see Table 6 highlighted Bold). This means that we cannot uniquely select a model that best describes the data in all mice.

5 Discussion

In this study, we developed within-host mathematical models of HBV infection that describe the mechanisms behind differences in viral kinetics between HEP mice (engrafted with human hepatocytes) and HEP/HIS mice (dually co-engrafted with human hepatocytes and components of a human immune system) Hogan et al. (2023). They are adaptations of previous within-host models developed for humans and chimpanzees infections Ciupe et al. (2007b, a) and all have key HBV-specific components. Specifically, given the hepatocyte tropism for HBV, a term describing fast liver proliferation following liver stress and death has been included Summers et al. (2003). Moreover, given that HBV is a DNA virus that does not always integrate in the genome of an infected cell, a cure of infected cells term has been considered Guidotti et al. (1999); Wieland et al. (2004). Lastly, given that HBV does not kill infected cells by itself, only immune-mediated infected cell death was considered Thimme et al. (2003).

We fitted the models with measured sHBV and HBsAg data from seven mice in HEP group and twelve mice in HEP/HIS group reported in Hogan et al. 2023 and estimated several key parameter values for each group. Since empirical data showed reduction in both sHBV and HBsAg in mice from HEP/HIS group compared to those in the HEP group Hogan et al. (2023), we assumed that the grafted human immune system mounts

an antiviral response against HBV. We determined inter group variability by assuming no antiviral responses for the HEP group (model Eq. 1 with $\delta = 0$) and modeling three possible immune functions for the HEP/HIS group: cytolytic immune responses leading to cell death (model Eq. 1 with $\delta \neq 0$); non-cytolytic immune responses leading to cure and refraction to reinfection of previously infected cells (model Eq. 6); and delayed non-specified antiviral effect reducing viral production weeks after infection (model Eq. 8).

We found similar dynamics for the seven mice in the HEP group, with fast expansion of sHBV (and HBsAg) reaching high equilibria of $6.7 \times 10^7 - 7.4 \times 10^8$ sHBV per ml ($2.7 \times 10^3 - 1.2 \times 10^4$ HBsAg per ml), $2-3$ weeks post infection. By contrast, there is large variability within the HEP/HIS group, regardless of which immune function is being modeled. All the models and data herein predict reduction in both sHBV and HBsAg levels. The magnitude of the HBsAg reduction is similar among models, reaching $2.7 - 7.7 \times 10^3$ copies per ml equilibrium for model Eq. 1, $2.7 - 6 \times 10^3$ copies per ml equilibrium for model Eq. 6 and $2-5 \times 10^3$ copies per ml equilibrium for model Eq. 8. The magnitude of the sHBV reduction, however, depends on the model considered, reaching $4.3 \times 10^5 - 2.3 \times 10^7$ copies per ml equilibrium for model Eq. 1, $10^3 - 8.33 \times 10^5$ copies per ml equilibrium for model Eq. 6 and $1.6 \times 10^4 - 2.1 \times 10^7$ copies per ml equilibrium for model Eq. 8. The time to reach sHBV equilibrium is 2-3 weeks for models Eq. 1 and Eq. 8 and one year for Eq. 6.

Our goal was to select the immune response model that best describes the data in the immune competent group HEP/HIS. Model Eq. 1 (with $\delta \neq 0$) predicted high percent liver loss (up to 95%) in some mice. That would lead to mice death, which is not in agreement with experimental data showing limited evidence of liver injury Hogan et al. (2023). Moreover, Eq. 1 predicts oscillatory behavior in some of the mice, which is not seen in set-point data. Hence Eq. 1 (with $\delta \neq 0$) can be eliminated. Model Eq. 8, which predicted that antiviral effects result in reduction of up to 99% viral production (one to three weeks post infection) best describe the data of nine mice (Table 6). This is reminiscent of a previous report on early acute hepatitis C virus kinetics in immuno competent chimpanzees Dahari et al. (2005). In the remaining three mice, both models Eqs. 8 and 6, which assumes non-cytolytic immune function with infected cells being cured and becoming refractory to reinfection, explain the data. Hence it is inconclusive if non-cytolytic immune responses, antiviral effects or a combination of the two is needed for reduction in the sHBV and serum HBsAg concentrations, as observed in the HEP/HIS mice.

Our study has several limitations. First, we assumed that the reduction in viral production happens instantaneously, and modeled it using a step function. A more realistic approach would be to model gradual decay based on non-hepatotoxic processes, such as interferon or lymphotoxin beta induced activation of cytidine deaminases acting on cccDNA. More data is needed to determine the shape of such a continuous antiviral effect and overall sHBV and HBsAg dynamics, which can have complex patterns of decay, as seen recently in HBV infected severe combined immunodeficient mice Hailegiorgis et al. (2023); Ishida et al. (2018). Second, we assumed that the immune processes are mutually exclusive. That is, of course, not the case and a combination of mechanisms may be responsible for the observed differences in the sHBV and HBsAg dynamics in the HEP and HEP/HIS groups. The sparcity of the data, however, pre-

vents us from modeling them at the same time. Lastly, we made several assumptions for our fixed parameters, who can influence our results. In particular, we assumed a long HBsAg half-life of 69 days (based on preliminary fitting). Previous work showed high variability in the estimates of the half-life of serum HBsAg, ranging from a few hours up to 38 days Neumann et al. (2010); Chulanov et al. (2003); Kadelka et al. (2021); Shekhtman et al. (2018); Hershkovich et al. (2023); Shekhtman et al. (2020). Future work is needed to determine whether the longer half-life is a characteristic of our animal model.

In conclusion, we have developed several within-host models of HBV infection and used them to predict which immune mechanisms led to a reduction in sHBV and HBsAg in HEP/HIS mice compared to HEP mice. We validated the models against experimental data and found that both non-cytolytic antiviral mechanisms (yet to be identified) that lead to large reduction in viral production 1-3 weeks after the infection and/or non-cytolytic infected cell cure that lead to the emergence of cells refractory to reinfection may be responsible for improved outcomes. Further experimental and theoretical efforts are needed to dissect the human immune response mechanisms of viral control that can guide interventions.

Supplementary Information The online version contains supplementary material available at https://doi.org/10.1007/s11538-024-01284-2.

Acknowledgements SMC was partially supported by NSF1813011, NSF2051820 and NIH NIGMS R01GM152743. HD was partially supported by NIH R01AI144112, R01AI158666 and R01AI146917. AP was partially supported by NIH R01AI138797, R01AI153236, R01AI146917, R01AI168048, Research Scholar Award from the American Cancer Society RSG-15-048-01-MPC, and by Burroughs Wellcome Fund Award for Investigators in Pathogenesis.

Data statement The code used in the manuscript and the data will be available on SMC github account uppon publication.

References

Asabe Shinichi, Wieland Stefan F, Chattopadhyay Pratip K, Roederer Mario, Engle Ronald E, Purcell Robert H, Chisari Francis V (2009) The size of the viral inoculum contributes to the outcome of hepatitis B virus infection. J Virol 83(19):9652–9662

Bertoletti Antonio, Gehring Adam J (2006) The immune response during hepatitis B virus infection. J Gen Virol 87(6):1439–1449

Billerbeck Eva, Mommersteeg Michiel C, Shlomai Amir, Xiao Jing W, Andrus Linda, Bhatta Ankit, Vercauteren Koen, Michailidis Eleftherios, Dorner Marcus, Krishnan Anuradha et al (2016) Humanized mice efficiently engrafted with fetal hepatoblasts and syngeneic immune cells develop human monocytes and NK cells. J Hepatol 65(2):334–343

Chulanov Vladimir P, Shipulin German A, Schaefer Stephan, Gerlich Wolfram H (2003) Kinetics of HBV DNA and HBsAg in acute hepatitis B patients with and without coinfection by other hepatitis viruses. J Med Virol 69(3):313–323

Ciupe Stanca M (2018) Modeling the dynamics of hepatitis B infection, immunity, and drug therapy. Immunol Rev 285(1):38–54

Ciupe Stanca M, Ribeiro Ruy M, Nelson Patrick W, Dusheiko Geoffrey, Perelson Alan S (2007) The role of cells refractory to productive infection in acute hepatitis B viral dynamics. Proc Natl Acad Sci 104(12):5050–5055

Ciupe Stanca M, Ribeiro Ruy M, Nelson Patrick W, Perelson Alan S (2007) Modeling the mechanisms of acute hepatitis B virus infection. J Theor Biol 247(1):23–35

Ciupe Stanca M, Ribeiro Ruy M, Perelson Alan S (2014) Antibody responses during hepatitis B viral infection. PLoS Comput Biol 10(7):e1003730

Ciupe Stanca M, Vaidya Naveen K, Forde Jonathan E (2021) Early events in hepatitis B infection: the role of inoculum dose. Proc R Soc B 288(1944):20202715

Dahari Harel, Major Marian, Zhang Xinan, Mihalik Kathleen, Rice Charles M, Perelson Alan S, Feinstone Stephen M, Neumann Avidan U (2005) Mathematical modeling of primary hepatitis C infection: noncytolytic clearance and early blockage of virion production. Gastroenterology 128(4):1056–1066

Dusséaux Mathilde, Masse-Ranson Guillemette, Darche Sylvie, Ahodantin James, Li Yan, Fiquet Oriane, Beaumont Elodie, Moreau Pierrick, Rivière Lise, Neuveut Christine et al (2017) Viral load affects the immune response to HBV in mice with humanized immune system and liver. Gastroenterology 153(6):1647–1661

Fang Zhong, Li Jin, Xiaoyu Yu, Zhang Dandan, Ren Guangxu, Shi Bisheng, Wang Cong, Kosinska Anna D, Wang Sen, Zhou Xiaohui et al (2015) Polarization of monocytic myeloid-derived suppressor cells by hepatitis B surface antigen is mediated via ERK/IL-6/STAT3 signaling feedback and restrains the activation of T cells in chronic hepatitis B virus infection. J Immunol 195(10):4873–4883

Ferrari CARLO, Penna A, Bertoletti A, Valli A, Delgi Antoni A, Giuberti TIZIANA, Cavalli ALBERTINA, ANNE Petit MARIE (1990) Cellular immune response to hepatitis B virus-encoded antigens in acute and chronic hepatitis B virus infection. J Invest Med 145(10):3442–3449

Forde Jonathan E, Ciupe Stanca M, Cintron-Arias Ariel, Lenhart Suzanne (2016) Optimal control of drug therapy in a hepatitis B model. Appl Sci 6(8):219

Glebe Dieter, Lorenz Heike, Gerlich Wolfram H, Butler Scott D, Tochkov Ilia A, Tennant BudC, Cote Paul, Menne Stephan (2009) Correlation of virus and host response markers with circulating immune complexes during acute and chronic woodchuck hepatitis virus infection. J Virol 83(4):1579–1591

Guidotti Luca G, Ishikawa Tetsuya, Hobbs Monte V, Matzke Brent, Schreiber Robert, Chisari Francis V (1996) Intracellular inactivation of the hepatitis B virus by cytotoxic T lymphocytes. Immunity 4(1):25–36

Guidotti Luca G, Rochford Rosemary, Chung Josan, Shapiro Max, Purcell Robert, Chisari Francis V (1999) Viral clearance without destruction of infected cells during acute HBV infection. Science 284(5415):825–829

Gutti Tanuja L, Knibbe Jaclyn S, Makarov Edward, Zhang Jinjin, Yannam Govardhana R, Gorantla Santhi, Sun Yimin, Mercer David F, Suemizu Hiroshi, Wisecarver James L et al (2014) Human hepatocytes and hematolymphoid dual reconstitution in treosulfan-conditioned uPA-NOG mice. Am J Pathol 184(1):101–109

Hailegiorgis Atesmachew, Ishida Yuji, Collier Nicholson, Imamura Michio, Shi Zhenzhen, Reinharz Vladimir, Tsuge Masataka, Barash Danny, Hiraga Nobuhiko, Yokomichi Hiroshi et al (2023) Modeling suggests that virion production cycles within individual cells is key to understanding acute hepatitis B virus infection kinetics. PLoS Comput Biol 19(8):e1011309

Hershkovich Leeor, Shekhtman Louis, Bazinet Michel, Pântea Victor, Placinta Gheorge, Cotler Scott J, Vaillant Andrew, Dahari Harel (2023) Rapid monophasic HBsAg decline during nucleic-acid polymer-based therapy predicts functional cure. Hepatol Commun 7(8):e0205

Hogan Glenn, Winer Benjamin Y, Ahodantin James, Sellau Julie, Huang Tiffany, Douam Florian, Funaki Masaya, Chiriboga Luis, Lishan Su, Ploss Alexander (2023) Persistent hepatitis B virus and HIV coinfections in dually humanized mice engrafted with human liver and immune system. J Med Virol 95(7):e28930

Ishida Yuji, Chung Tje Lin, Imamura Michio, Hiraga Nobuhiko, Sen Suranjana, Yokomichi Hiroshi, Tateno Chise, Canini Laetitia, Perelson Alan S, Uprichard Susan L et al (2018) Acute hepatitis B virus infection in humanized chimeric mice has multiphasic viral kinetics. Hepatology 68(2):473–484

Kadelka Sarah, Dahari Harel, Ciupe Stanca M (2021) Understanding the antiviral effects of rnai-based therapy in HBeAg-positive chronic hepatitis B infection. Sci Rep 11(1):200

Kim Jin Hyang, Ghosh Alip, Ayithan Natarajan, Romani Sara, Khanam Arshi, Park Jang-June, Rijnbrand Rene, Tang Lydia, Sofia Michael J, Kottilil Shyam et al (2020) Circulating serum hbsag level is a biomarker for HBV-specific T and B cell responses in chronic hepatitis B patients. Sci Rep 10(1):1835

McClary Heike, Koch Rick, Chisari Francis V, Guidotti Luca G (2000) Relative sensitivity of hepatitis B virus and other hepatotropic viruses to the antiviral effects of cytokines. J Virol 74(5):2255–2264

Monolix version 2019r2. Antony, France: Lixoft SAS, (2019)

Murray John M, Purcell Robert H, Wieland Stefan F (2006) The half-life of hepatitis B virions. Hepatology 44(5):1117–1121

Murray John M, Wieland Stefan F, Purcell Robert H, Chisari Francis V (2005) Dynamics of hepatitis B virus clearance in chimpanzees. Proc Natl Acad Sci 102(49):17780–17785

Neumann Avidan U, Phillips Sandra, Levine Idit, Ijaz Samreen, Dahari Harel, Eren Rachel, Dagan Shlomo, Naoumov Nikolai V (2010) Novel mechanism of antibodies to hepatitis B virus in blocking viral particle release from cells. Hepatology 52(3):875–885

Rath S, Devey Madeleine E (1988) IgG subclass composition of antibodies to hbsag in circulating immune complexes from patients with hepatitis B virus infections. Clin Exp Immunol 72(1):164

Shekhtman L, Borochov N, Cotler S, Hershkovich L, Uprichard S, Al-Mahtab M, Bazinet M, Vaillant A, Dahari H (2018) Modeling serum HBsAg, HBV DNA and transaminase kinetics during REP 2139 monotherapy in chronic HBeAg+ HBV infection. J Hepatol 68:S508

Shekhtman Louis, Cotler Scott J, Hershkovich Leeor, Uprichard Susan L, Bazinet Michel, Pantea Victor, Cebotarescu Valentin, Cojuhari Lilia, Jimbei Pavlina, Krawczyk Adalbert et al (2020) Modelling hepatitis D virus RNA and HBsAg dynamics during nucleic acid polymer monotherapy suggest rapid turnover of HBsAg. Sci Rep 10(1):7837

Summers Jesse, Jilbert Allison R, Yang Wengang, Aldrich Carol E, Saputelli Jeffry, Litwin Samuel, Toll Eugene, Mason William S (2003) Hepatocyte turnover during resolution of a transient hepadnaviral infection. Proc Natl Acad Sci 100(20):11652–11659

Thimme Robert, Wieland Stefan, Steiger Carola, Ghrayeb John, Reimann Keith A, Purcell Robert H, Chisari Francis V (2003) CD8+ T cells mediate viral clearance and disease pathogenesis during acute hepatitis B virus infection. J Virol 77(1):68–76

Whalley Simon A, Murray John M, Brown Dave, Webster George JM, Emery Vincent C, Dusheiko Geoffrey M, Perelson Alan S (2001) Kinetics of acute hepatitis B virus infection in humans. J Exp Med 193(7):847–854

Wieland Stefan F, Spangenberg Hans Christian, Thimme Robert, Purcell Robert H, Chisari Francis V (2004) Expansion and contraction of the hepatitis B virus transcriptional template in infected chimpanzees. Proc Natl Acad Sci 101(7):2129–2134